# Optical Vortices in Self-Focusing Kerr Nonlinear Media

Peter Hansinger[a], Alexander Dreischuh[*,b], Gerhard G. Paulus[a]

[a]*Institute for Optics and Quantum Electronics, Friedrich-Schiller-University, Max-Wien-Platz 1, D-07743 Jena, Germany*
[b] *Department of Quantum Electronics, Sofia University, 5, J. Bourchier Blvd., Sofia-1164, Bulgaria*

**Abstract**

In this work we numerically compare the interaction of optical vortices (OVs) in self-defocusing and self-focusing Kerr nonlinear media. We find that the basic scenarios (attraction/repulsion, translation/rotation vs. background) in the interaction of two and three vortices with equal and alternative topological charges (TCs) are the same in both media. However, the vortex dynamics under self-focusing conditions is influenced by the reshaping of the surrounding part of the background. Square structure of OVs with alternating TCs is found to be stable with respect to the vortex positions in self-focusing media. This elementary cell is successfully generalized in a large square array of OVs with alternative TCs which brings ordering in the multiple filamentation of the background beam in self-focusing conditions.

*Key words:* Kerr nonlinearity, self-focusing, optical vortex, vortex interaction, filamentation, vortex array
*PACS:* 42.65.-k, 42.65.Jx, 42.65.Sf, 42.65.Tg

## 1. Introduction

The presence of phase dislocations in the wavefront of a light beam determines its phase and intensity structure. Since the phase becomes indeterminate at singularity points, both the real and the imaginary parts of the field amplitude (i.e. also the field intensity) vanish [1]. An isolated point singularity with a screw-type phase distribution is associated with an optical

*Corresponding author. Tel.: (+359 2) 8161 611; fax: (+359 2) 868 88 13.
*Email address:* `ald@phys.uni-sofia.bg` (Alexander Dreischuh)

vortex (OV). The characteristic helical phase profiles of OVs are described by $\exp(im\varphi)$ multipliers, where $\varphi$ is the azimuthal coordinate and the integer number $m$ is their topological charge (TC). The study of OVs has received special attention in recent years not only because of their rich linear and nonlinear dynamics [2, 3, 4, 5, 6, 7], but also due to a variety of potential applications including particle micro-manipulation [8], imaging [9], interferometry [10], and quantum information [11].

Singular nonlinear optics [12] will benefit from ultrashort pulses carrying spatial phase dislocations, since such pulses exhibit peak intensities high enough to access optical nonlinearities in many materials. The methods for creating OVs (and other singular beams) in femtosecond pulses are already established. Possible approaches include optical systems utilizing computer generated holograms or a spatial light modulator aligned within optical schemes with spatial dispersion compensation: a dispersionless $4f$- [13, 14, 15] or $2f-2f$-setup [16], or a double-pass grating compressor [13]. An achromatic vortex lens comprising pair of suitable adjacent optical glasses whose interface resembles a helicoid seems to be able to create an OV free of topological dispersion [17]. Polychromatic OVs (and OV solitons) are also generated by uniaxial crystals [18, 19].

Despite the large activities in defocusing nonlinear materials, the dynamics of beams with such complex phase structure in self-focusing nonlinear media has remained weakly explored. As self-focusing materials are more common in nature, this is somewhat surprising and could be explained by the intrinsic beams' azimuthal and modulational instabilities [20, 21, 22, 23]. Only recently stable spiraling bound state of two vortices of the same TC are found in nonlocal self-focusing nonlinear media [24]. In self-defocusing Kerr media, in contrast, the basic interaction scenarios between OVs are well understood (see e.g. [2, 3, 25]) and stable vortex lattices are demonstrated [26, 27, 28]. In this work we model numerically and compare the interaction of optical vortices in local self-defocusing and self-focusing Kerr nonlinear media searching for rotational and translational rigid OV lattice which, under self-focusing conditions, can bring ordering in the multiple filamentation of the background beam and can provide the necessary refractive index modulation for off-site guiding of ordered probe beams.

## 2. Numerical procedure

The numerical simulations of the OVs propagation along the nonlinear medium (NLM) are carried out using the (2+1)-dimensional nonlinear Schrödinger equation (NLSE)

$$i\frac{\partial A}{\partial(z/L_{Diff})}+\frac{1}{2}\Delta_T A+sign(n_2)\frac{L_{Diff}}{L_{NL}}|A|^2A=0, \tag{1}$$

which accounts for the evolution of the slowly-varying optical beam envelope $A$ influenced by nonlinearity and diffraction. In the NLSE $\Delta_T$ is the transverse part of the Laplace operator whereas $L_{Diff}=kr_0^2$ and $L_{NL}=1/(k|n_2|I)$ stand for the diffraction and nonlinear length of the beam and $sign(n_2)=\pm 1$ for self-focusing and self-defocusing Kerr nonlinearity respectively. ($sign(n_2)=1$ and $L_{Diff}=L_{NL}$ is the necessary condition for bright spatial soliton formation). In the above notations, $k$ is the wave number in the medium and $I$ is the peak field intensity. The transverse spatial coordinates (e.g. $x$ and $y$) are normalized to the OV beam width $r_0$. We solved the NLSE by means of the beam propagation method with a computational window spanning over $1024\times 1024$ grid points. The input OV is described by

$$A=A_0B(r)\tanh(r/r_0)\exp(im\varphi) \tag{2}$$

where $A_0$ is the peak field amplitude, $B(r)$ is the super-Gaussian bright background carrying the dark beams ($B(r)=\exp\{-(r^2/r_{BG}^2)^8\}$; $r_{BG}=0.64\times 512 pix.$), $\tanh(r/r_0)$ describes the OV profile ($r_0=14.7pix.$) and the integer $m$ is the OV TC. The background beam was chosen sufficiently broad to avoid any interaction of the OVs with its gradients. As a standard test we modelled the formation of a single-charged optical vortex soliton (OVS) (see Fig. 1). If not stated otherwise, the intensity in the simulations is kept equal to that needed to form a charge-one OVS ($I=I_{SOL}^{OV}$).

## 3. Vortex pair interaction

It is known that a pair of singly-charged OVs with the same sign of the TCs rotate on the background and repel each other, whereas OVs of opposite TCs attract each other (eventually annihilating) and translate with respect to the background. We will first concentrate on the comparison between the vortex-pair dynamics in self-focusing ($n_2>0$) and self-defocusing ($n_2<0$) NLM (see Figs. 2 and 3) for equal TCs. Due to background-beam instability

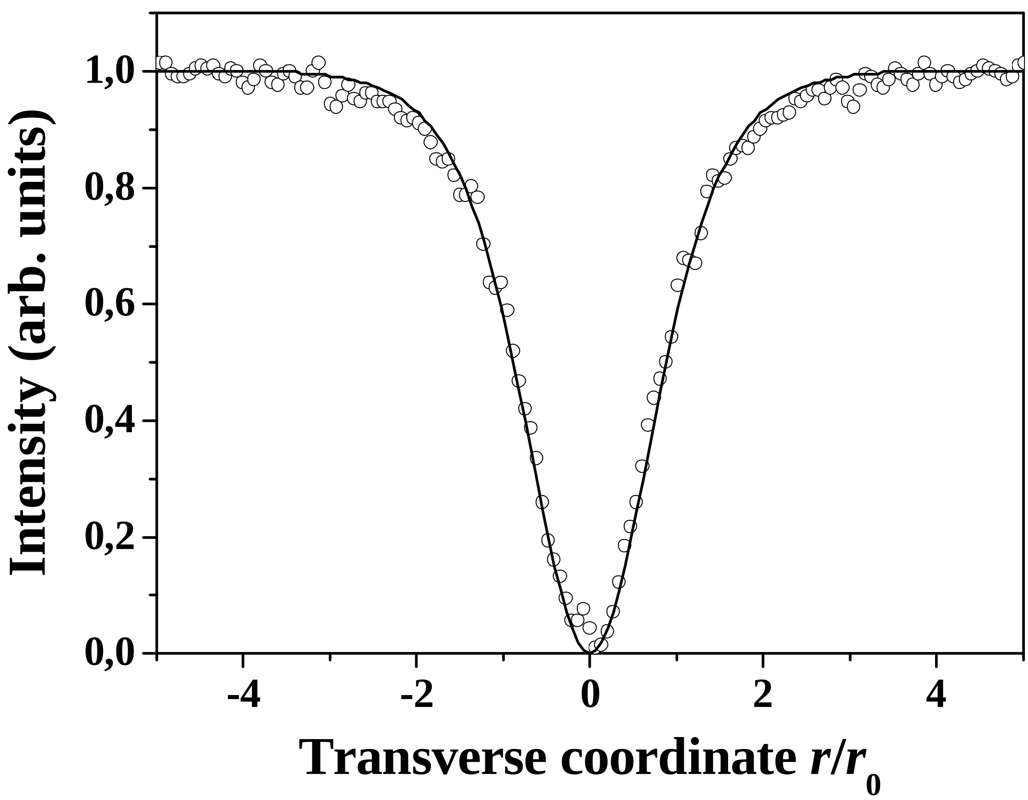


Figure 1: Cross-section of the input OV beam (solid curve) and the fundamental OV soliton formed at $z = 4L_{NL}$ (open circles).

and self-focusing, a valid comparison between the two nonlinear regimes is limited to propagation lengths $z = 2L_{NL}$ as indicated by vertical dotted lines in Fig. 2. The evolution of the OVs in the self-defocusing regime is typically followed up to $z = 5L_{NL}$. The correct identification of the position of the screw phase dislocation within the dark OV core is done by inspecting the OV phase profiles. In Fig. 2 we show the vortex pair rotation angle (a) and the distance between the vortices (b) as a function of the nonlinear propagation length $z/L_{NL}$. Curves referring to the self-focusing regime of propagation are easily identified by their termination prior/at $z/L_{NL} = 2$ (see the vertical dotted line). Open circles and dashed curves refer to self-defocusing nonlinearity, whereas solid circles and solid curves correspond to $n_2 > 0$. Initial vortex-to-vortex distances of $42pix.$ and $28pix.$ are considered. In the self-defocusing regime, as expected, the closer the vortices the stronger their interaction. This is especially well pronounced in the OV pair rotation

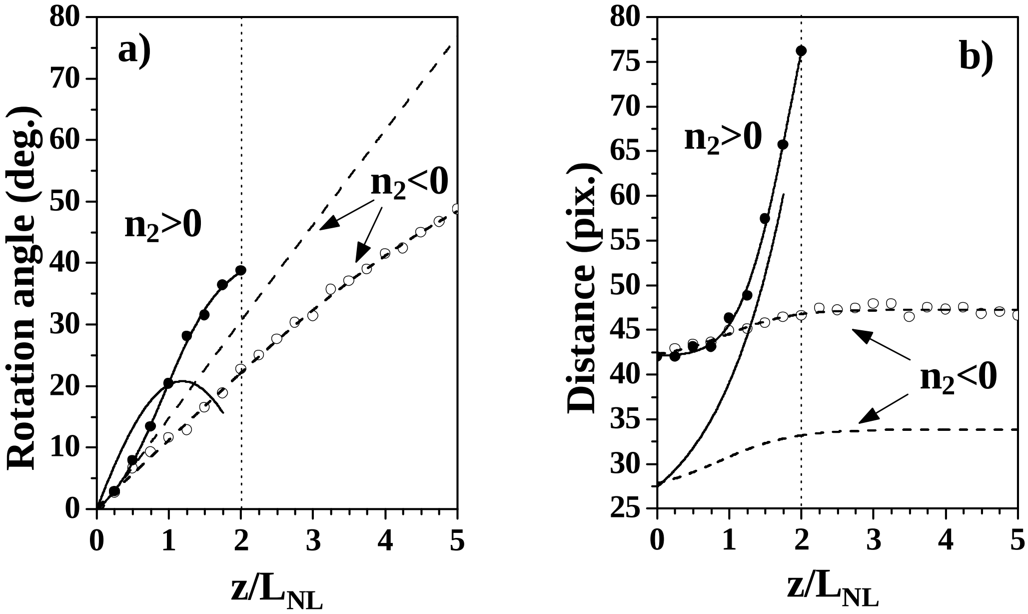


Figure 2: Equal TCs. Vortex pair rotation angle (a) and distance between the vortices (b) vs. nonlinear propagation length. Open circles and dashed lines refer to self-defocusing nonlinearity, solid circles and solid curves correspond to $n_2 > 0$. Initial vortex-to-vortex distances $42pix.$ (open/solid circles) and $28pix.$ (curves with no symbols).

angle (Fig. 2a, dashed curves) but can be also recognized in the relative increase of the vortex-to-vortex distance (Fig. 2b, dashed curves). The first impression from the vortex dynamics in the self-focusing regime is that, under comparable initial conditions, it is initially much stronger as compared to the dynamics in the case of $n_2 < 0$. This behaviour, particularly visible in the vortex-to-vortex distance vs. nonlinear propagation length, we attribute to the fact that for $n_2 > 0$ the vortex cores spread out much stronger as compared to the linear regime, overlap considerably and the interaction is stronger (see Fig. 3). The same is true during the initial stage of the OV pair rotation (see Fig. 2a) but , in contrast to the case in [24], the background-beam modulation and self-focusing at larger propagation distances (see the right frame in Fig. 3) forces the rotation speed to decrease and even to reverse (Fig. 2a, pure solid curve). The conclusion which can be drawn at this point for equally charged OVs is that under comparable initial conditions the change in the sign of the nonlinearity from negative to positive increases the OV pair dynamics keeping the general interaction scenario unchanged.

It is known that in self-defocusing nonlinear media OVs of opposite TCs

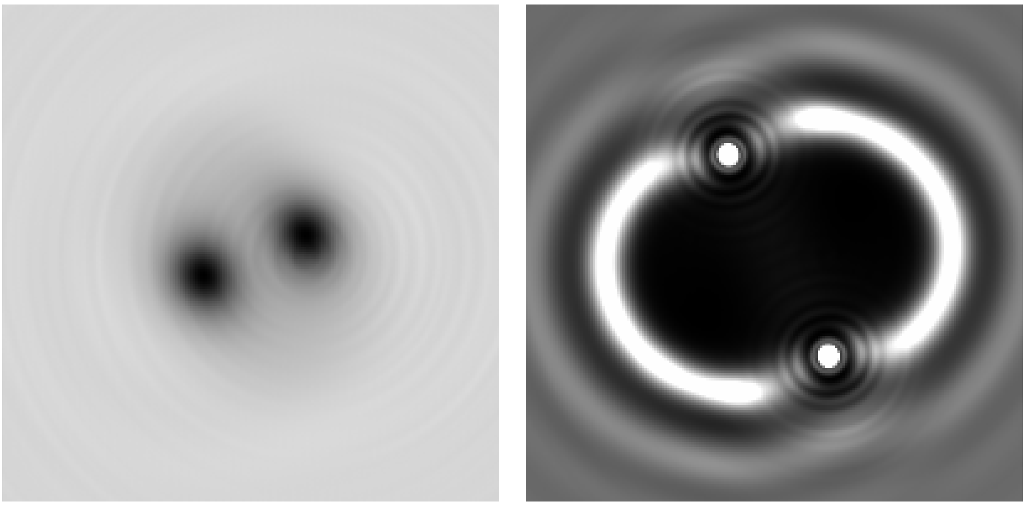

Figure 3: OV pairs of equal TCs at $z = 2L_{NL}$ for negative (left) and positive Kerr nonlinearity (right). Initial vortex-to-vortex distance $42pix$. The effects of self-focusing require a bigger dynamic range for the right panel, in this case 2.5 times. In reality the intensity of the background in both cases would be comparable. Some 3.8% of the total computational area are shown.

attract each other (eventually annihilating at a certain propagation distance) and translate on the background parallel to the imaginary line connecting the vortex cores. The numerical results shown in Fig. 4a for $n_2 < 0$ clearly confirm that the vortex pair translation with respect to the background increases linearly with the propagation distance. The transverse velocity of the vortex pair is higher for initially more closely spaced OVs. We also find the vortex-to-vortex distance to decrease monotonically at a rate that depends on the reciprocal value of the vortex initial separation (see the dashed curves in Fig. 4b). The most striking difference observed numerically in the self-focusing case under comparable initial conditions is that the oppositely charged OVs drift rapidly in opposite directions (see the solid curves in Fig. 4b). The calculated curves end at propagation distances at which the self-focusing peak (lying symmetrically with respect to the OVs, see the right frame in Fig. 5) reaches 8 times the initial field amplitude. This peak strongly modulates the background between the OVs and, prevailing over the pure topological interaction, effectively pushes the OVs away. The steep increase in the vortex-to-vortex separation should be expected to saturate at later evolution stages due to the surrounding self-focusing bright structure (Fig. 5, right frame), however we refrained from continuing the numerical cal-

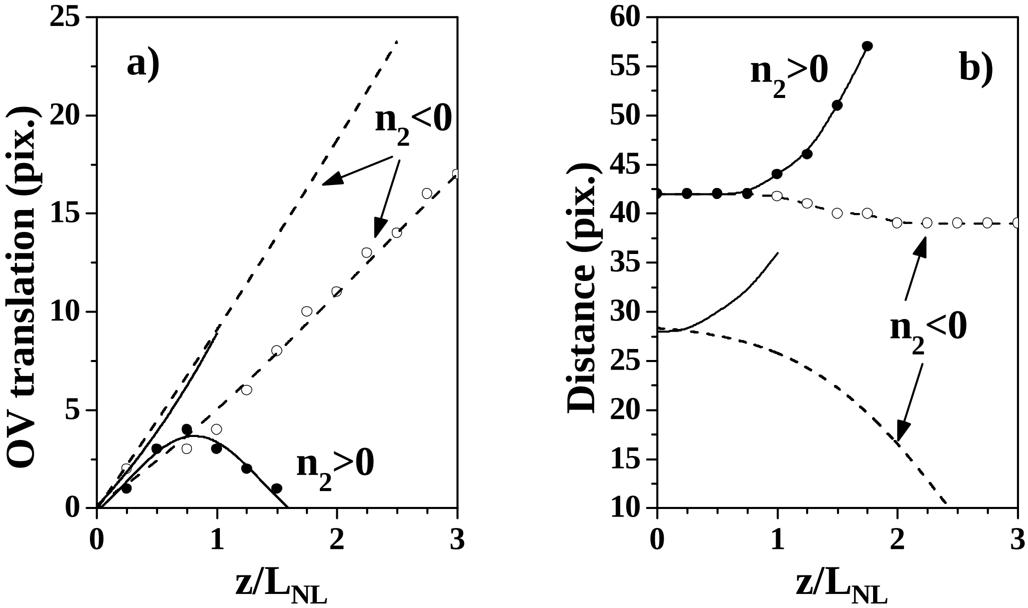


Figure 4: Opposite TCs. Vortex pair shift (a) and vortex-to-vortex distance (b) vs. nonlinear propagation length. Open circles and dashed lines refer to self-defocusing nonlinearity, solid circles and solid curves correspond to $n_2 > 0$. Initial vortex-to-vortex distances $42pix.$ (open/solid circles) and $28pix.$ (curves with no symbols).

culation since the used slowly-varying amplitude approximation of the NLSE is invalid in this regime. The initial tendency in the optical vortex shift (parallel translation) vs. propagation length at $n_2 > 0$ is qualitatively similar to the behaviour in the self-defocusing case, see the solid curves in Fig. 4a. At later stages however, the widely spaced OVs, which further are pushed apart by the self-focusing peak in between, start interacting with the surrounding self-focusing ellipse-like structure and the shift of the OV pair decreases and can even reverse. At this stage one can conclude that the general tendency that the closer the OVs the stronger their interaction does not depend on the particular sign of the Kerr nonlinearity. The bright structures self-focusing on the background beam have profound impact on the OV pair dynamics at $n_2 > 0$.

## 4. Linear structures of optical vortices

As a next step we modeled the behaviour of a linear structure of three equidistant single-charged OVs. The obtained numerical data for equally-

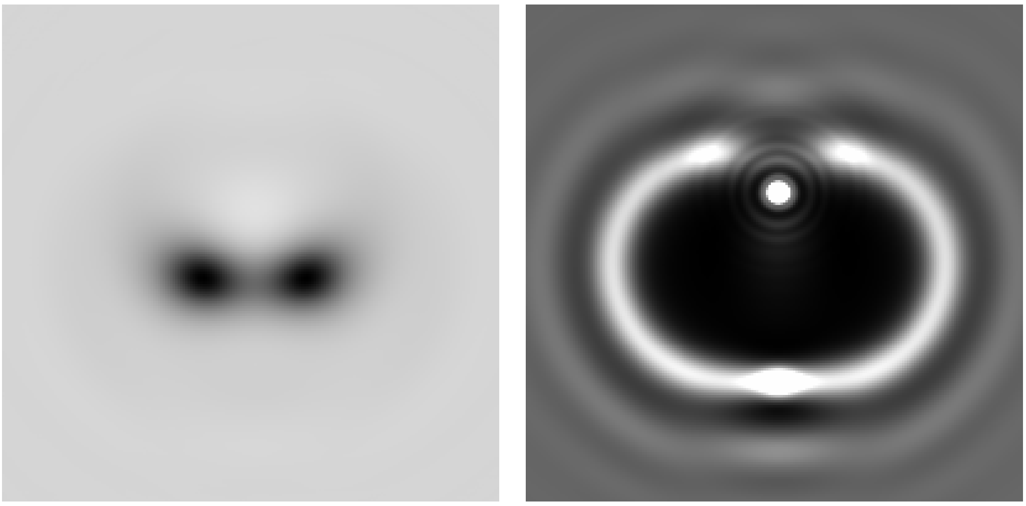

Figure 5: Opposite TCs. OV pairs at $z = 1.75L_{NL}$ for negative (left) and positive Kerr nonlinearity (right). Initial vortex-to-vortex distances $42pix$. For better visibility the gray scale for the right frame corresponds to a 2.5 times bigger dynamic range. Some 3.8% of the total computational area are shown.

charged OVs are summarized in Figs. 6 and 7, whereas Figs. 8 and 9 show the results for alternating TCs. The comparison of the data in Fig. 2a and Fig. 6a shows that the rotation of the linear array of three OVs is slower as compared to the case of an OV pair when the TCs are equal. This is true for $n_2 > 0$ and $n_2 < 0$ and for both inter-vortex distances used. Because of the influence of the relatively complicated self-focusing surrounding structure (see the right frame in Fig. 7) there is again a tendency of a decrease (and even a reversing sign) of the rotation speed vs. propagation length. For $n_2 < 0$ the repulsion of two and three equally charged OVs is almost linear up to $z = 2L_{NL}$. At $5L_{NL}$ the repulsion is the same for both signs of the nonlinearities (within the $1 - pix.$ resolution in the calculated phase distributions). For $n_2 > 0$ the repulsion of the OV pair is again stronger than the one between the three OVs. Again one can conclude that, in general, in both self-focusing and defocusing media the dynamics of three aligned equally-charged OVs is qualitatively similar to this of the OV pair of equal TCs.

The new behaviour observed with three OVs of alternative TCs is that the modulation and self-focusing of the background is so strong (see the lower left frame in Fig. 9) that the attraction between the two OVs is completely suppressed for $n_2 < 0$ and reversed to repulsion for $n_2 > 0$ (see Fig. 8b, solid curves). In case of a structure with an initial inter-vortex distance of

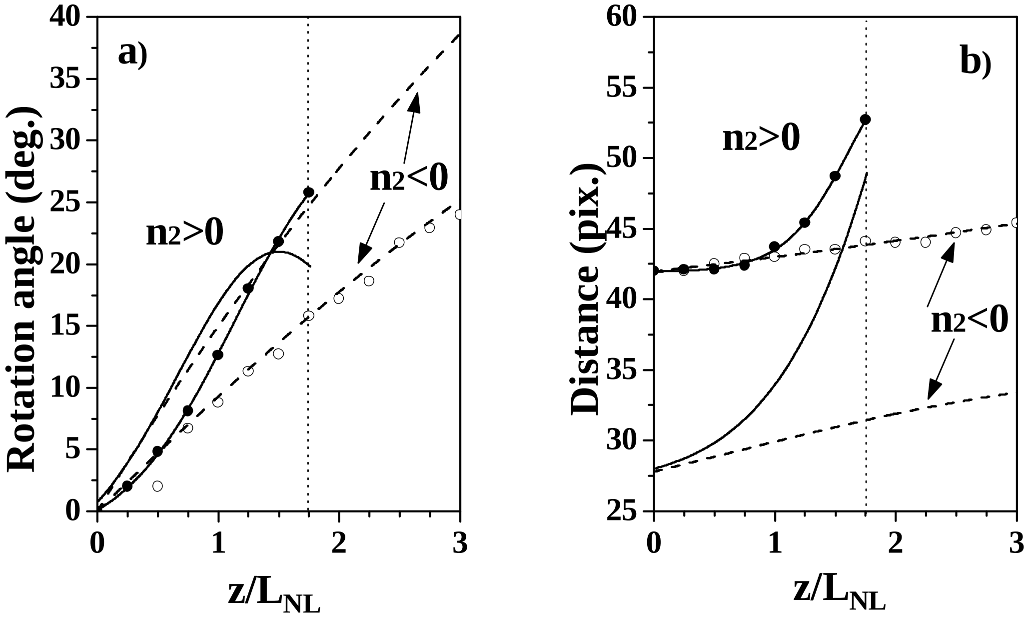


Figure 6: Three OVs with equal TCs. Rotation angle (a) and distance between two of the vortices (b) vs. nonlinear propagation length. Open circles and dashed lines refer to self-defocusing nonlinearity, solid circles and solid curves correspond to $n_2 > 0$. Initial vortex-to-vortex distances $42pix.$ (open/solid circles) and $28pix.$ (curves with no symbols).

$42pix.$, for $n_2 > 0$, the rotational angle is even reversed in sign (see the solid curve with solid dots in Fig. 8a). Interestingly, for the shorter initial inter-vortex distance of $28pix.$ we numerically observed clear annihilation of two of the oppositely-charged OVs. The intensity and phase profiles of the resulting dark structures are shown in Fig. 9. The arrows in the phase profiles indicate the position of the only OV surviving the vortex pair annihilation. Besides the effects of attraction/repulsion and shift/rotation, it is interesting to see whether for alternating TCs there is a change in the rotation speed of this simple structure for $n_2 > 0$ as expected for $n_2 < 0$. Let us therefore inspect the results for $n_2 > 0$ more closely. For the linear structure of three OVs of equal TCs, the rotation angle at $z/L_{NL} = 1.5$ is 22° for the initial $42 - pix.$ vortex-to-vortex distance and 20.5° for the $28 - pix.$ initial distance. The respective values of the rotation angle for the structure with alternating TCs are $-4.5°$ for the $42 - pix.$ structure and 16.5° for the $28 - pix.$ structure. This confirms the qualitative expectation that the TC of the middle OV has a noticeable influence on the rotation dynamics of the ensemble also for self-focusing conditions.

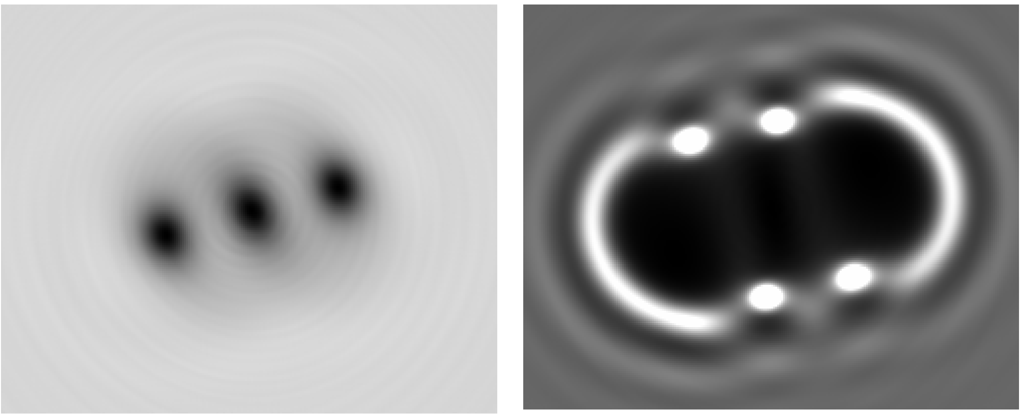

Figure 7: Equal TCs. Three OVs at $z = 1.75L_{NL}$ for negative (left) and positive Kerr nonlinearity (right). Initial vortex-to-vortex distances $42pix$. For better visibility the gray scale for the right frame corresponds to a 2.5 times bigger dynamic range. Some 4.6% of the total computational area are shown.

When the middle OV is doubly-charged (and its TC is opposite to those of the other vortices), the central vortex is not in its ground state. It decays into two singly-charged OVs of the same TC which strongly repel each other. The oppositely-charged OVs start to interact pairwise while translating in parallel on the background beam. This is observed to be well pronounced when following the dynamics of the structure in a self-defocusing NLM. The results shown in the upper row in Fig. 10 clearly demonstrate this at $z = 5L_{NL}$. For self-focusing conditions (Fig. 10, lower row), the vortex dynamics is qualitatively similar, although it is strongly influenced by self-focusing of the surrounding structure. This is evident when comparing the phase profiles of the structures (see Fig. 10, right column), in which the arrows indicate the positions of the vortices. For $n_2 > 0$ annihilation of the OV pairs was observed at a propagation distance of $z \sim 2L_{NL}$. All data shown in Fig. 10 refer to an initial OV-to-OV distance of $42pix$. For the shorter inter-vortex distance of $28pix.$, the observed behavior is qualitatively the same. However, the repulsion between the sub-products of the decayed central OV clearly dominates the pairwise interaction of the OVs, including annihilation for $n_2 > 0$ taking place at $z \sim 1.25L_{NL}$.

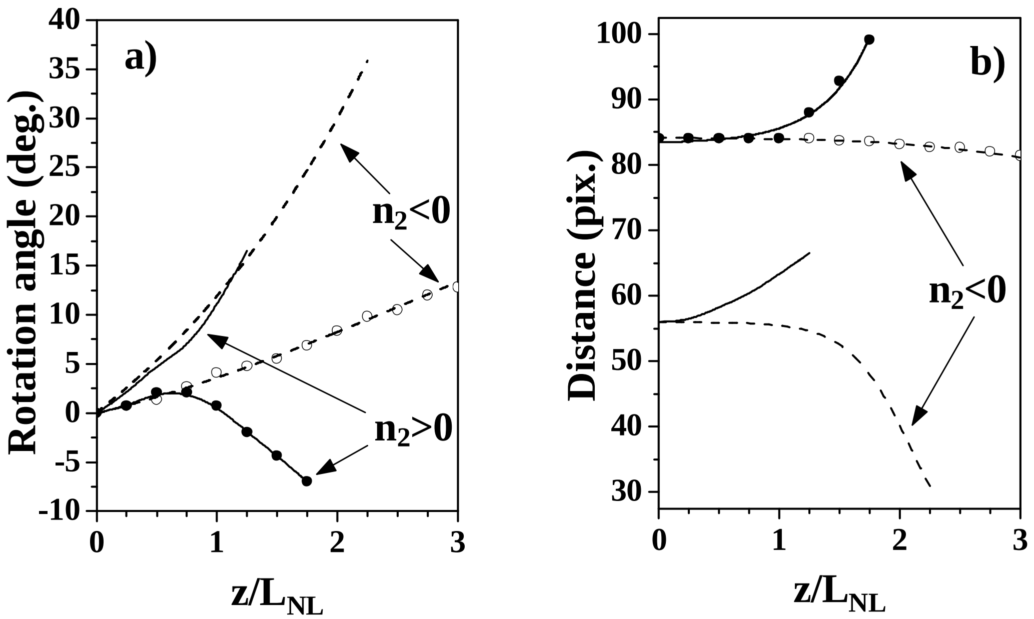


Figure 8: Three in-line OVs with alternating TCs. Rotation angle (a) and distance between the two outer vortices (b) vs. nonlinear propagation length. Open circles and dashed lines refer to self-defocusing nonlinearity, solid circles and solid curves correspond to $n_2 > 0$. Initial vortex structure length $2 \times 42pix.$ (open/solid circles) and $2 \times 28pix.$ (no symbols).

## 5. Square optical vortex array

The next more complicated configuration, namely four OVs situated in the apices of a square with alternating TCs of the OVs, is referred to as an *optical leopard* [29]. The nonlinear evolution of this configuration in self-defocusing Kerr NLM is well described in [30]. It has been found there that if such an ensemble is considered as consisting of two OV pairs with zero effective TC, after some nonlinear propagation length the two pairs of OVs exchange their interaction partners. In this way it has been shown that the coherent interaction of OVSs is elastic. In Fig. 11 we show the intensity and phase profile of the ensemble of four OVs with alternative TCs after a propagation distance $z = 1L_{NL}$ in a self-focusing NLM. Within an accuracy of $1pix.$ in estimating the vortex positions, we found that the vortices keep their initial positions and the influence of self-focusing of the background in a shamrock-like structure prevails the pairwise topological interaction observed in self-defocusing NLM.

The rigid behaviour of this ensemble motivated us to consider it as an

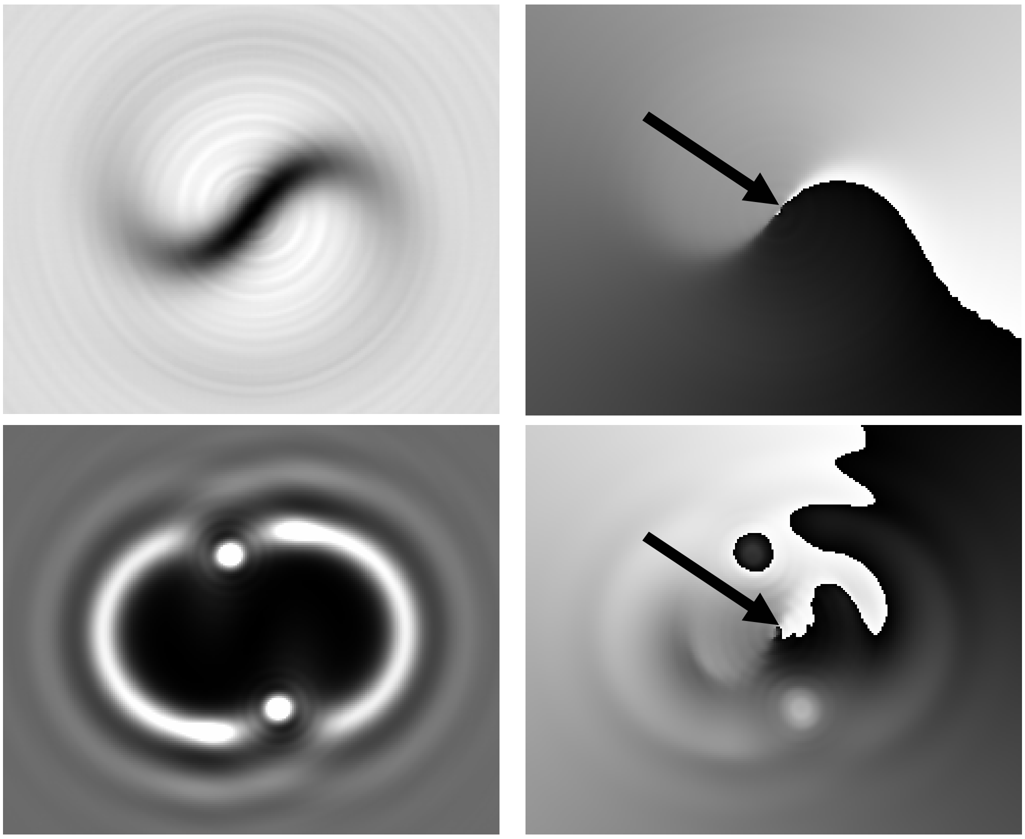

Figure 9: Alternating TCs. Three OVs at $z = 1.75L_{NL}$ for negative (upper row) and positive Kerr nonlinearity (lower row). Initial vortex-to-vortex distances $42pix$. For better visibility the gray scale for the lower left frame is 2.5 times higher than this for the upper left frame. Some 4.6% of the total computational area are shown.

elementary cell of a large square array of OVs with alternating TCs which, if stable, could bring ordering, for instance, in the filamentation of intense laser beams in self-focusing NLM. Previous experimental and numerical results in self-defocusing NLM showed [27] that such a square optical lattice is stable and is able to induce in the nonlinear medium periodic modulation of the refractive index, which is sufficiently strong to force a probe beam to diffract by it. In view of the similar basic interaction scenarios for OVs in self-focusing and self-defocusing NLM (attraction/repulsion, transverse translation/rotation) and the results shown in Fig. 11, it is intriguing to see whether the stability of the large square lattice of OVs holds also under self-focusing conditions. In Fig. 12 we show numerical results obtained with a large array of some 600 OVs ordered in a square matrix with inter-vortex distance of $42pix$. Fig. 12a demonstrates the typical texture-like structure formed on the initially flat-toped background beam after a linear propagation to $z = 5L_{Diff}$. In our view this structure is a result of the paarwise interaction of oppositely charged OVs. The background beam intensity in the nonlinear regimes was set to $I = 1.268I_{SOL}^{OV}$ in order to compensate for the reduction in the effective intensity between the vortices due to the overlapping of their wings. (This coefficient depends on the particular ratio of the OV-to-OV distance to the individual OV beam width $r_0$). Under self-defocusing conditions (Fig. 12b) the distance between the OVs in the central part of the array, over several grating periods, was measured to be exactly $42pix.$ as set initially. In the self-defocusing wings of the background beam the vortex-to-vortex distance was found to increase up to $\sim 60pix.$ due to the interaction with the finite background. These estimations were made by inspecting the phase profile of the vortex array. In order to measure adequately the position of the self-focusing bright peaks (Fig. 12c) we stretched the greyscale of the computed image 10 times. We measured that the distances between the bright filaments are exactly $42pix.$ at $z = 1.5L_{NL}$, even in the peripheral part of the background beam. This is identical to the initial OV-to-OV distance. In order to get a basis for comparison, the results shown in Fig. 12 use the same grey scales. In this mode of the presentation one can see that self-focusing is weaker in the peripheral areas as a result of lower background intensity. In addition, the low-intensity cross-sections of the self-focused filaments are slightly elliptical, whereas their high-intensity cross sections are circular. The weak ellipticity in the low-intensity cross sections of the filaments we attribute to the texture-like structure resulting from the OV topological interactions (Fig. 12a). In case of an OV lattice of a smaller grating constant ($28pix.$) we observed a stronger texture-like structure in the linear regime. During self-focusing of the beam we observed the development of ordered sub-structures in self-focusing filaments. In our view this violates the slowly varying envelope approximation and we will refrain to speculate on it.

## 6. Conclusion

The behaviour of optical vortices and optical vortex arrays has been reviewed and investigated in both self-defocusing and self-focusing Kerr nonlinear media. The interaction scenarios between two vortices (attraction/repulsion, transverse shift/rotation) in both cases are qualitatively similar. However, in the self-focusing regime the interaction (repulsion, rotation, shift) is enhanced and in some cases even reversed in sign. This can be explained by the influence of reshaping the background beam, which then affects the interaction between the vortices significantly.

Those basic results were generalized to more complex structures, namely three in a line vortices and for vortices on a square. It was found that the square lattice array of vortices with alternating topological charge will develop into an ordered structure of filaments in the self-focusing case. The mutual attraction of adjacent vortices with different topological charge in conjunction with the reshaping of the background beam due to self-focusing gives rise to a stable propagation of the lattice-like structure with the bright filaments located off-site in between the vortex cores. Although the model presented here does not include any temporal effects and others like saturation of the nonlinearity (i.e. via ionization), we believe that vortices can in principle be used as a means of spatial control in the filamentation of high-intense laser pulses in Kerr nonlinear media.

## 7. Acknowledgments

The authors gratefully acknowledges funding by the DFG in the framework of Forschergruppe 532 “Nichtlineare raum-zeitliche Dynamik in dissipativen und diskreten optischen Systemen”. A.D. is grateful to the Institute of Optics and Quantum Electronics, FSU-Jena, Germany, for the warm hospitality during his research stay. This work was supported by the National Science Foundation (NSF)-Bulgaria, project $DO - 02 - 0114/2008$.

## References

[1] J. F. Nye, M. V. Berry, Proc. R. Soc. London A 336 (1974) 165–190.

[2] Yu. S. Kivshar, B. Luther-Davies, Phys. Rep. 298 (1998) 81–197.

[3] A. S. Desyatnikov, Yu. S. Kivshar, L. Torner, in *Progress in Optics*, 47, Ed. E. Wolf (North-Holland, Amsterdam, 2005) 291–391.

[4] G. A. Swartzlander, Jr., C. T. Law, Phys. Rev. Lett. 69 (1992) 2503–2506.

[5] Z. Chen, M.-F. Shih, M. Segev, D. W. Wilson, R. E. Muller, P. D. Maker, Opt. Lett. 22 (1997) 1751–1753.

[6] A. H. Carlsson, J. N. Malmberg, D. Anderson, M. Lisak, E. A. Ostrovskaya, T. J. Alexander, Yu. S. Kivshar, Opt. Lett. 25 (2000) 660–662.

[7] C. T. Law, X. Zhang, G. A. Swartzlander, Jr., Opt. Lett. 25 (2000) 55–57.

[8] D. G. Grier, Nature 424 (2003) 810–816.

[9] G. Foo, D. M. Palacios, G. A. Swartzlander, Jr., Opt. Lett. 30 (2005) 3308–3310.

[10] S. Furhapter, A. Jesacher, S. Bernet, M. Ritsch Marte, Opt. Lett. 30 (2005) 1953–1955.

[11] G. Molina Terriza, J. P. Torres, L. Torner, Nature Physics 3 (2007) 305–310.

[12] M. S. Soskin, M. V. Vasnetsov, in *Progress in Optics*, 42, Ed. E. Wolf (North-Holland, Amsterdam, 2001) 219–276.

[13] K. Besuchanov, A. Dreischuh, G. G. Paulus, M. G. Schätzel, H. Walther, D. Neshev, W. Krolikowski, Yu. Kivshar, J. Opt. Soc. Am. B 23 (2006) 26–35.

[14] K. Besuchanov, A. Dreischuh, M. G. Schätzel, G.G. Paulus, H. Walther, Opt. Lett. 29 (2004) 1942–1944.

[15] I. Zeylikovich, H. I. Sztul, V. Kartazaev, T. Le, R. R. Alfano, Opt. Lett. 32 (2007) 2025–2027.

[16] I. G. Mariyenko, J. Strohaber, C. J. G. J. Uiterwaal, Optics Express 13 (2005) 7599–7608.

[17] G. A. Swartzlander, Jr., Opt. Lett. 31 (2006) 2042–2044.

[18] D. N. Neshev, A. Dreischuh, V. Shvedov, A. S. Desyatnikov, W. Krolikowski, Yu. S. Kivshar, Opt. Lett. 33 (2008) 1851–1853.

[19] A. Volyar, V. Shvedov, T. Fadeyeva, A. S. Desyatnikov, D. N. Neshev, W. Krolikowski, Yu. S. Kivshar, Optics Express 14 (2006) 3724–3729.

[20] V. Tikhonenko, J. Christou, B. Luther-Davies, J. Opt. Soc. Am. B 12 (1995) 2046–2052.

[21] W. J. Firth, D. V. Skryabin, Phys. Rev. Lett. 79 (1997) 2450–2453.

[22] L. Torner, D. V. Petrov, Electron. Lett. 33 (1997) 608–610.

[23] L. T. Vuong, T. D. Grow, A. Ishaaya, A. L. Gaeta, G. W. Hooft, 't, E. R. Eliel, G. Fibich, Phys. Rev. Lett. 96 (2006) 133901–4.

[24] D. Buccoliero, A. S. Desyatnikov, W. Krolikowski, Yu. S. Kivshar, Opt. Lett. 33 (2008) 198–200.

[25] D. Rozas, C. T. Law, G. A. Swartzlander, Jr., J. Opt. Soc. Am. B 14 (1997) 3054–3065.

[26] D. Neshev, A. Dreischuh, M. Assa, S. Dinev, Opt. Commun. 151 (1998) 413–421.

[27] A. Dreischuh, S. Chervenkov, D. Neshev, G. G. Paulus, H. Walther, J. Opt. Soc. Am. B 19 (2002) 550–556.

[28] A. S. Desyatnikov, N. Sagemerten, R. Fisher, B. Terhalle, D. Träger, D. N. Neshev, A. Dreischuh, C. Denz, W. Krolikowski, Yu. S. Kivshar, Optics Express 14 (2006) 2851–2863.

[29] C. O. Weiss, H. R. Telle, K. Staliunas, M. Brambilla, Phys. Rev. A 47 (1993) R1616–R1619.

[30] K. Staliunas, Chaos, Solitons and Fractals 4 (1994) 1783–1796.

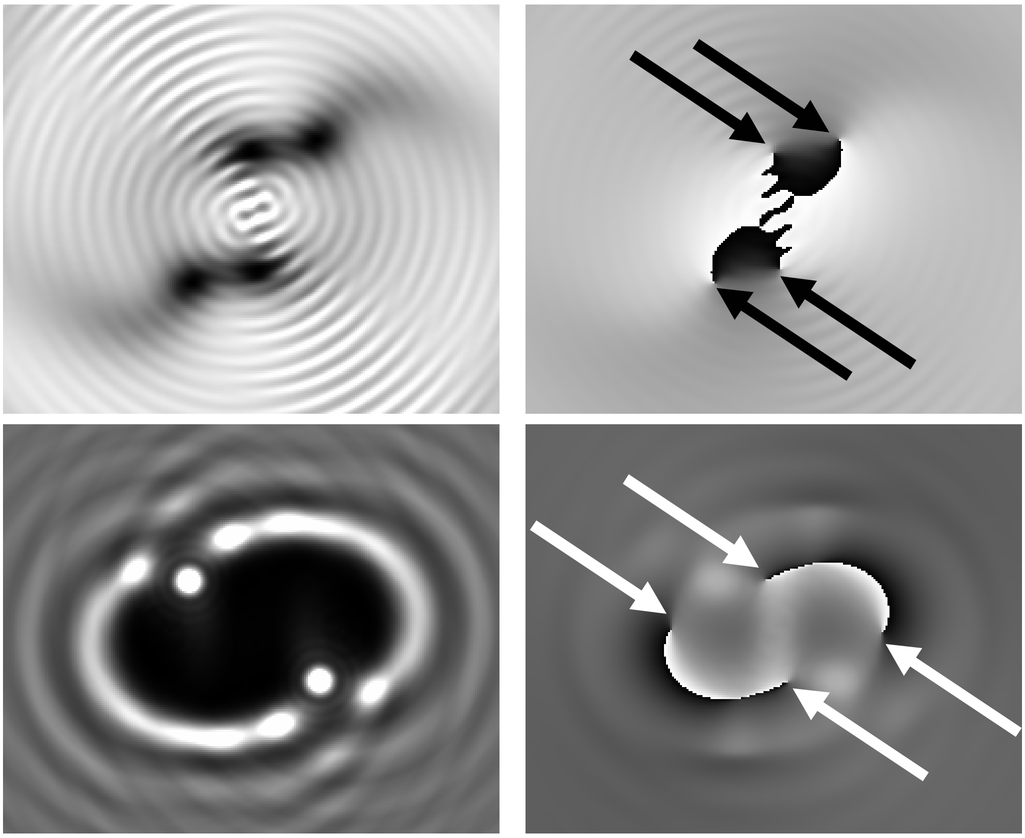

Figure 10: Middle OV double-charged oppositely to the side-lying OVs. Intensity (left) and phase profiles (right) at $z = 5L_{NL}$ for negative (upper row) and at $z = 1.5L_{NL}$ for positive Kerr nonlinearity (lower row). Initial vortex-to-vortex distances $42pix$. The gray scale for the lower left frame is 2 times higher than this for the upper left frame. The arrows in the phase profiles indicate the cores of the vortices. Some 4.6% of the total computational area are shown.

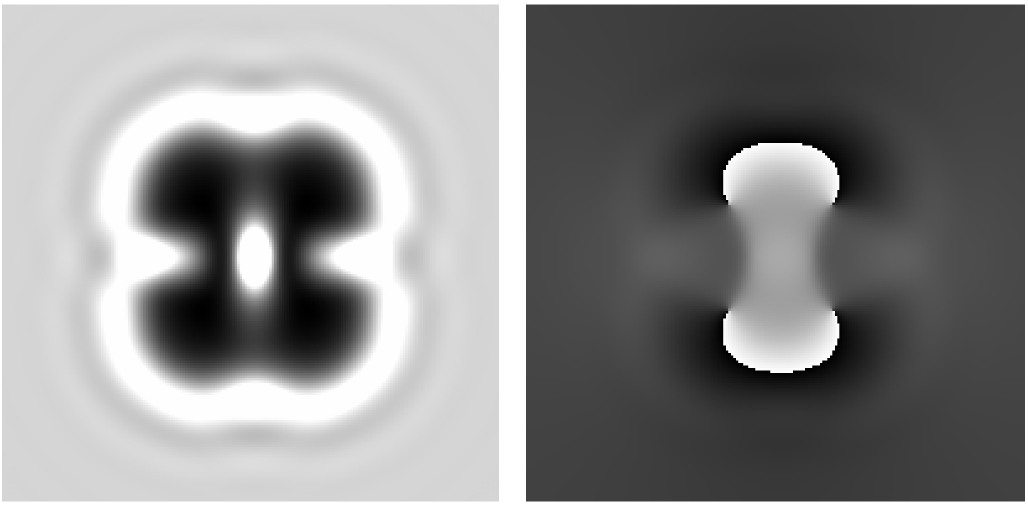

Figure 11: Four OVs with alternating TCs. Intensity (left) and phase profile (right) at $z = 1L_{NL}$ for positive Kerr nonlinearity. Initial vortex-to-vortex distances $42pix$. Some 3.8% of the total computational area are shown.

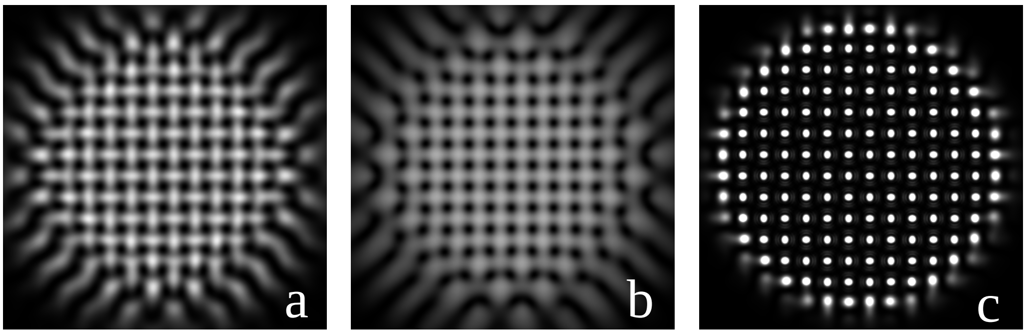


Figure 12: Large rectangular array of OVs at OV-to-OV distance $42pix$. Linear evolution (a) and propagation in self-defocusing regime (b) up to $z = 5L_{NL}$. Ordered multiple filaments created off-site with respect to the vortex array in self-focusing regime at $z = 1.5L_{NL}$ (c). In the nonlinear regimes $I = 1.268I_{SOL}^{OV}$. 40% of the total computational area are shown.